

Europa: Disk-Resolved Ultraviolet Measurements Using the Galileo Ultraviolet Spectrometer

A. R. Hendrix, C. A. Barth, and C. W. Hord

Laboratory for Atmospheric and Space Physics, University of Colorado, 1234 Innovation Drive, Boulder, Colorado 80309-0590
E-mail: hendrix@colorado.edu

and

A. L. Lane

Jet Propulsion Laboratory, California Institute of Technology, 4800 Oak Grove Drive, Pasadena, California 91109-8009

Received September 8, 1997; revised January 8, 1998

The Galileo ultraviolet spectrometer has measured the first-ever disk-resolved spectral ultraviolet albedos of regions on Europa's trailing and antijovian hemispheres at spatial resolutions approaching 55 km. We find that the ultraviolet albedo (2400–3200 Å) increases with distance from the trailing hemisphere apex (270° W). Regions close to 270° W display an absorption feature centered near 2800 Å, which generally decreases with distance from the trailing hemisphere apex. These results substantiate the idea that magnetospheric bombardment darkens the surface of the entire trailing hemisphere and creates an absorber in the central portion of the trailing hemisphere. The absorption is related to sulfur, but is much darker than any laboratory spectra, likely due to the large grain size on Europa's trailing hemisphere. The disk-resolved observations, in combination with three disk-integrated observations, are used to derive the ultraviolet particle scattering function for Europa's trailing hemisphere. © 1998 Academic Press

Key Words: Europa; Galileo spacecraft; spectroscopy; ultraviolet observations.

1. INTRODUCTION

Galileo has been in orbit around Jupiter since December 1995. In the intervening time, the ultraviolet spectrometer on board has performed many observations of the Galilean satellite Europa. Previous observations of Europa have included measurements by the Voyager spacecraft, Earth-based measurements by IUE and HST, and ground-based measurements. The observations reported here are unique because they represent the first-ever disk-resolved ultraviolet spectra of this icy surface. We explain what these spectra reveal about Europa's surface and its environment.

Background

The surface of Europa is significantly affected by the environment of this icy satellite which is phase-locked with

Jupiter, so that one side (centered on 0° longitude) always faces Jupiter. The leading hemisphere is centered on 90° longitude, while the central longitude of the trailing hemisphere is 270°. The trailing hemisphere has long been known to be darker than the leading hemisphere at ultraviolet, visible and infrared wavelengths (Stebbins 1927, Stebbins and Jacobsen 1928, Millis and Thompson 1975, Morrison *et al.* 1974, Johnson *et al.* 1983, McEwen 1986, Nelson *et al.* 1986, Nelson *et al.* 1987). This hemispheric dichotomy is likely due to two exogenic sources: magnetospheric bombardment on the trailing hemisphere and preferential bombardment of the leading hemisphere by micrometeorites.

Bombardment by Jupiter's corotating magnetosphere preferentially affects the trailing hemisphere and leads to alteration of particle size, sputtering, and implantation of species. Smaller grains on Europa's trailing hemisphere surface may be preferentially destroyed by this bombardment (Johnson *et al.* 1988, Calvin *et al.* 1995), creating an overall darker surface. Sputtering may cause material to be lost to space or to be redeposited elsewhere on the surface (Sieveka and Johnson 1982). Sputtering is likely the source of Europa's recently detected ionosphere (Kliore *et al.* 1997).

Exogenic processes that may affect the brightness of Europa's jovian hemisphere are bombardment by neutral particles emanating from Io and/or charged dust from Jupiter's gossamer ring (Hamilton 1996). Io is another likely source of dust in the Jupiter system, where dust particles are emitted in the volcanic eruptions and escape Io, streaming radially outward (Horanyi 1996). Neutral wind bombardment has been suggested as a possible source of an absorption feature found on Callisto's jovian hemisphere, as detected by IUE (Lane and Domingue 1997), and as the source of the IUE-measured change in brightness in Europa's jovian hemisphere in the past decade (Domingue and Lane 1997).

Absorption features have been detected on Europa's trailing hemisphere that do not appear on the leading hemisphere, causing researchers to conclude that an exogenic process is at work. The absorption features have been correlated with location on Europa's surface in relation to the trailing hemisphere apex. Disk-integrated observations with IUE (Lane *et al.* 1981, Ockert *et al.* 1987), HST (Noll *et al.* 1995), and the Galileo ultraviolet spectrometer (Hendrix *et al.* 1996) have shown that Europa's trailing hemisphere exhibits an absorption feature centered near 2800 Å. This feature has been attributed to an interaction between S and O atoms within the water ice lattice caused by sulfur ions from Io's torus being swept up by Jupiter's magnetosphere and implanted into the surface of Europa's trailing hemisphere (Lane *et al.* 1981). Noll *et al.* (1995) discussed the possibility that sulfur on Europa is endogenic in origin and is exposed on the trailing hemisphere when magnetospheric bombardment erodes away the icy upper layer. Domingue and Lane (1997) demonstrated the longitudinal variation in the 2800 Å feature using disk-integrated IUE measurements at several longitudes. The absorption feature was found in albedos measured in the 225°–255°, 255°–285°, and 285°–315° W longitude regions, and it was noticeably absent in leading hemisphere longitude bins. Pospieszalska and Johnson (1989) showed how implantation of magnetospheric ions (particularly S⁺) varies with the cosine of the angle from the trailing hemisphere pole (270° longitude); this pattern was correlated with Voyager-measured ratios of ultraviolet (0.35 μm) albedo to orange (0.59 μm) albedo. McEwen (1986) used Voyager images in several filters to show how the albedo of Europa varies with the cosine of the angle (latitude or longitude) from the trailing hemisphere apex. He found that the Voyager global mosaic UV/VIS image was dominated by an exogenically formed elliptic dark region over the trailing hemisphere. The ultraviolet (0.35 ± 0.03 μm) albedo was not as sensitive to endogenic albedo features as at longer wavelengths, and no obvious latitudinal dependence in the ultraviolet albedo was found. Johnson *et al.* (1988) detected an absorption feature in the Voyager UV filter (attributed to an H–S or S–S band) that was directly correlated with the ion bombardment longitudinal distribution and attributed the darkening in all filters toward the trailing hemisphere apex with an increase in grain size.

This Research

We present disk-resolved ultraviolet spectral measurements of Europa's surface, as measured by the Galileo ultraviolet spectrometer (UVS). These measurements, with spatial resolutions between 740 and 55 km, allow us to begin to understand variations in the ultraviolet albedo of Europa's trailing hemisphere with longitude, latitude, and terrain type. We first develop an ultraviolet phase

curve for Europa's trailing hemisphere to correct for observational geometry. We discuss the variation of Europa's ultraviolet albedo across the trailing hemisphere and the exogenic processes that may have caused these variations. We also map the ultraviolet absorption band, previously measured only in global observations, as it varies over the trailing hemisphere, and we investigate the nature of Europa's trailing hemisphere dark terrain.

These new data are significant because they are the first-ever disk-resolved observations of Europa's surface at near-ultraviolet wavelengths. Our data generally agree with the Voyager results (described above), and we find interesting variations in the ultraviolet absorption band not detectable from Voyager.

2. DATA

The Galileo Ultraviolet Spectrometer

The Galileo UVS was built at the University of Colorado's Laboratory for Atmospheric and Space Physics and is described in Hord *et al.* (1992). It consists of a Cassegrain telescope used to collect light and an Ebert–Fastie scanning spectrometer. A diffraction grating scans the ultraviolet spectrum and three photomultiplier tubes record the signal. All data reported here were acquired using the F channel, which covers the 1620–3231 Å wavelength region with a spectral resolution of 13.7 Å. The calibration of the F channel is described in Hendrix (1996). The entire spectrum is scanned in 4.33 sec, with a 0.006-sec integration period for each of the 528 grating positions. The angular size of the slit is 0.1° × 0.4°.

The UVS has the capability of taking spectra in a recording mode and in a real-time mode. The real-time spectra are summed together and cannot be separated into individual spectra; thus, real-time data do not provide the spatial information that recorded data offer.

Figure 1 displays the location and relative size of the field-of-view (FOV) on Europa during each observation. Figure 1 includes Galileo SSI camera images (J. Granahan, personal communication), which aid in the understanding of the terrains observed. The observations are summarized in Table I, where we indicate the latitude and longitude of the boresight of the slit, the size of the area observed, the viewing geometry (α , μ , μ_0) averaged over the slit at the time of the observation, and the number of spectra acquired (at 4.33 sec per spectrum), as well as the operating mode (record or real-time) for each observation.

3. METHOD

To intercompare the measured brightnesses from the regions observed, analysis of the UVS Europa data included the removal of the radiation background, division by the solar spectrum, and correction for viewing geometry

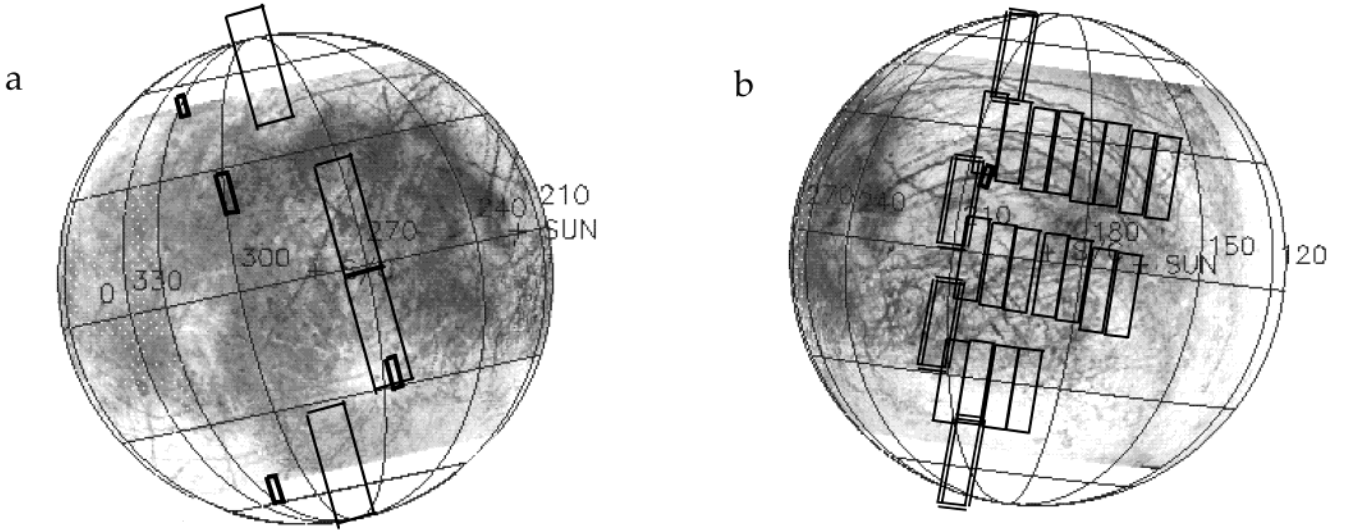


FIG. 1. Approximate location and UVS field-of-view (FOV) size during each of the disk-resolved Europa observations. Spectra that were used to obtain albedos for these regions came from around this region, not only from exact region shown by FOV footprints. (See Table I for additional observational geometry information.) (a) ASTERI observation (larger FOVs), E4 SUCOMP01, SUCOMP02, SUCOMP03, E6 SUCOMP01 observations. (b) TERRA INCOGNITA observation (double-lined FOVs), FLEXUS observation, E6 SUCOMP02 observation (small FOV).

by using a simplified Hapke photometric function (Hapke 1981).

Radiation Background Removal

The radiation background level is significant at Europa's orbit ($9.4 R_J$). In all of the UVS spectra, the measured signal below 2000 \AA was approximately flat, indicating that the reflected solar spectrum from Europa's surface was negligible. For each spectrum, we averaged the number of counts between 1620 and 2000 \AA and subtracted that amount from each spectrum as background radiation. After subtracting the background, we found that the signal was generally strong for wavelengths longer than 2200 – 2500 \AA . Table II displays the subtracted radiation background for each observation sequence. (Each observation within a sequence had approximately the same value of background radiation removed.)

Photometric Function for Disk-Resolved Observations

In order to compare all of the disk-resolved observations to each other, the data were reduced and corrections were made for the phase, emission, and incidence angles using a simplified version of the Hapke function (Hapke 1981)

$$r_m(\mu, \mu_0, \alpha, \lambda) = \omega(\lambda) \frac{\mu_0}{\mu + \mu_0} [p(\alpha, b, c) + H(\mu)H(\mu_0) - 1], \quad (1)$$

where we solved for the single-scatter albedo $\omega(\lambda)$.

In Eq. (1), μ and μ_0 refer to the cosine of the emission and incidence angles, respectively, and r_m is the measured reflectance (calibrated data/solar spectrum); SOLSTICE-measured solar spectra (Rottman *et al.* 1993), measured on the days of the Galileo observations, were used with these Europa data to divide out the reflected solar features. Comparisons between Europa data from different orbits should not be affected by variations in the solar spectrum. Figure 2 displays the ratios of solar spectra from the different days studied here; the greatest variation in flux is less than 1.5%. Multiple scattering is taken into account by including an approximation for the Chandrasekhar H functions, $H(\mu)$ and $H(\mu_0)$ (Hapke 1981).

The phase function used in this analysis was a double-lobed Henyey–Greenstein particle phase function

$$p(\alpha, b, c) = \frac{(1-c)(1-b^2)}{(1+2b \cos \alpha + b^2)^{3/2}} + \frac{c(1-b^2)}{(1-2b \cos \alpha + b^2)^{3/2}}, \quad (2)$$

where b and c are the scattering parameters, which describe how backward or forward scattering a particle is. Equation (2) and the b and c parameters are described in Domingue *et al.* (1991). The b parameter describes the width of the scattering lobe, while c describes the amplitude. For the phase function of Eq. (2), the half-widths of the forward and backward scattering lobes are the same, while the amplitude of each may be different.

Because the ultraviolet particle phase function of Euro-

TABLE I
Summary of UVS Disk-Resolved Observations

Observation	Latitude	Longitude	α^a	μ^a	μ_0^a	Footprint (km)	Number of spectra	Operating mode ^b
E4 SUCOMP01	53° S	318° W	61°	0.54	0.23	27 × 107	38	rec.
E4 SUCOMP02	26° N	299° W	58°	0.88	0.54	48 × 193	23	rec.
E4 SUCOMP03	54° N	321° W	73°	0.45	0.19	14 × 54	63	rec.
ASTERI 1	47° N	287° W	56°	0.58	0.29	185 × 739	14	RT
ASTERI 2	13° N	271° W	56°	0.92	0.71	182 × 728	14	RT
ASTERI 3	16° S	271° W	56°	0.91	0.71	180 × 719	14	RT
ASTERI 4	49° S	286° W	56°	0.58	0.32	178 × 713	14	RT
E6 SUCOMP01	26° S	266° W	40°	0.71	0.20	28 × 112	55	rec.
E6 SUCOMP02	16° N	208° W	52°	0.74	0.93	18 × 70	55	rec.
TERINC 1	54° N	205° W	36°	0.56	0.50	172 × 689	14	RT
TERINC 2	12° N	209° W	36°	0.96	0.79	167 × 667	14	RT
TERINC 3	20° S	211° W	36°	0.92	0.75	161 × 645	14	RT
TERINC 4	59° S	211° W	36°	0.52	0.44	156 × 623	14	RT
FLEXUS Swath 1	29° N	207° W	22°	0.83	0.68	157 × 627	14	rec.
	29° N	200° W	22°	0.86	0.75	156 × 624	14	rec.
	28° N	193° W	22°	0.88	0.80	155 × 621	14	rec.
	28° N	186° W	22°	0.88	0.84	155 × 619	14	rec.
	27° N	180° W	22°	0.87	0.87	154 × 616	14	rec.
	27° N	173° W	22°	0.85	0.89	153 × 613	14	rec.
	26° N	167° W	22°	0.82	0.90	153 × 611	14	rec.
	26° N	160° W	22°	0.77	0.89	152 × 608	14	rec.
	0° N	203° W	21°	0.98	0.83	151 × 606	14	rec.
	1° S	197° W	21°	0.99	0.89	151 × 603	14	rec.
FLEXUS Swath 2	1° S	191° W	21°	0.99	0.93	151 × 600	14	rec.
	1° S	185° W	21°	0.99	0.96	149 × 598	14	rec.
	1° S	180° W	21°	0.98	0.98	149 × 595	14	rec.
	2° S	174° W	21°	0.96	0.99	148 × 593	14	rec.
	2° S	168° W	21°	0.92	0.99	148 × 590	14	rec.
	28° S	209° W	21°	0.83	0.69	147 × 587	14	rec.
FLEXUS Swath 3	28° S	202° W	21°	0.86	0.75	146 × 585	14	rec.
	28° S	196° W	21°	0.88	0.80	146 × 582	14	rec.
	28° S	190° W	21°	0.88	0.83	146 × 580	14	rec.

Note. E4 and E6 refer to orbits 4 and 6, respectively. SUCOMP, SURface COMPosition; TERINC, TERRA INCOGNITA.

^a α = phase angle; μ = cos (emission angle); μ_0 = cos (incidence angle).

^b rec., record; RT, real-time.

pa's surface was unknown, the parameters b and c were derived using UVS data. To derive the ultraviolet particle phase function of Europa's trailing hemisphere, we used all of the UVS disk-resolved observations for longitudes

TABLE II
Background Radiation Levels

Observation	R_j	Average background radiation (counts/6 msec)
E4 SUCOMP01	9.3	1050
E4 SUCOMP02	9.25	1423
E4 SUCOMP03	9.36	675
E6 SUCOMP01	9.61	598
E6 SUCOMP02	9.54	537
FLEXUS	10.72	340
ASTERI	9.23	880
TERRA INCOGNITA	10.7	175

between 180° and 360° W and three disk-integrated trailing hemisphere observations (central longitudes of 315°, 225°, and 200° at phase angles of 79°, 58°, and 41°, respectively) to solve for best-fit ultraviolet values of b and c . This data set did not include observations at phase angles smaller than 21° or greater than 80°. We solved for the values of ω , b , and c for which χ^2 was a minimum, where

$$\chi^2 = \sum \frac{(r_m - r_c(\alpha, \mu, \mu_0, b, c, \omega))^2}{n}. \quad (3)$$

In Eq. (3), r_m is the measured reflectance and r_c is the reflectance calculated using the Hapke model (Eq. (1)); n is the number of observations. At 2900 Å, where the instrument's effective sensitivity (product of solar spectrum and spectral sensitivity) is at its peak, the best-fit values of b and c were found to be $b = 0.37$ and $c = 1.0$. Values of b and c were also derived at several additional

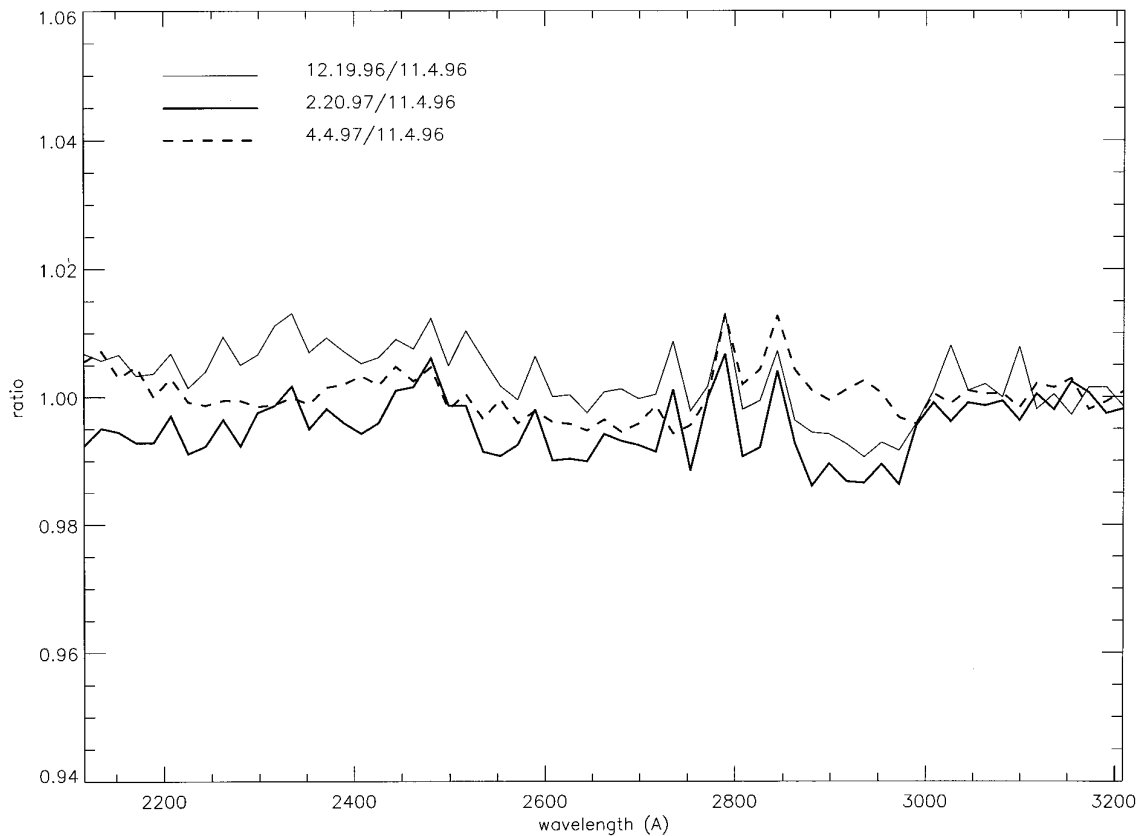


FIG. 2. Ratios of SOLSTICE-measured solar spectra (G. Rottman, personal communication) from the four different days during which Europa data were taken for this study. The solar spectrum from December 19, 1996, corresponds to the data obtained during the E4 orbit; the spectrum from February 20, 1997, corresponds to the E6 observations; the spectrum from April 4, 1997, corresponds to the data from the seventh orbit. Each of these spectra are shown ratioed to the solar spectrum from November 4, 1996, which is the date on which the Europa leading hemisphere disk-integrated albedo was measured and to which the disk-resolved trailing hemisphere albedos are ratioed in Fig. 5. The greatest variation in solar flux is less than 1.5%; therefore, we expect negligible effects from solar variation on Europa's albedo over the time period studied here.

wavelengths between 2300 and 3200 Å; variations in these derived parameters that affected the albedos significantly (more than statistical error) were not found, so the 2900 Å b and c values were used at all wavelengths. The derived ultraviolet phase function is shown in Fig. 3.

The derived phase function was used in Eq. (1) to solve for the single-scatter albedo (ω) of each observed region. Because we used the same phase function parameters for the data from each of the regions observed, this is a possible source of error in our results, as it is unknown how the different terrains we have observed vary in their backscattering properties in the near-ultraviolet. Domingue and Hapke (1992) determined that various europian terrains have b values (at 0.47 μm) generally around 0.35–0.40, with a single minimum value of 0.05. The c values for different terrains on Europa at 0.47 μm were determined by Domingue and Hapke (1992) to vary between 0.90 and 0.30.

We chose to neglect the opposition effect term, as Europa's surface has been found to have a negligible ultraviolet opposition surge (Buratti *et al.* 1988). Furthermore, it is

unknown what the ultraviolet Hapke parameters that represent the opposition effect are for any region on Europa, and Galileo data at very small phase angles do not yet exist to determine these parameters. Europa has been found to have a very minor opposition effect at visible wavelengths due to shadow hiding (Domingue *et al.* 1991), presumably because the bright surface creates multiple scattering that dilutes shadows; however, recent observations (Rosenbush *et al.* 1997) indicate that Europa's opposition effect is due to coherent backscatter. Therefore, it is not clear how much of Europa's opposition effect is due to shadow-hiding and how much is due to coherent backscatter. Domingue and Hapke (1992) used identical Hapke opposition effect terms in their photometric function when determining best-fit photometric parameters for several europian terrains using Voyager images, so it is not unreasonable to assume that the different terrains analyzed in this study have similar opposition surges, if any at all.

Surface roughness was also not taken into account. Although we are using data in the phase angle range ($\alpha > 20^\circ$) where surface roughness has an effect, we note that

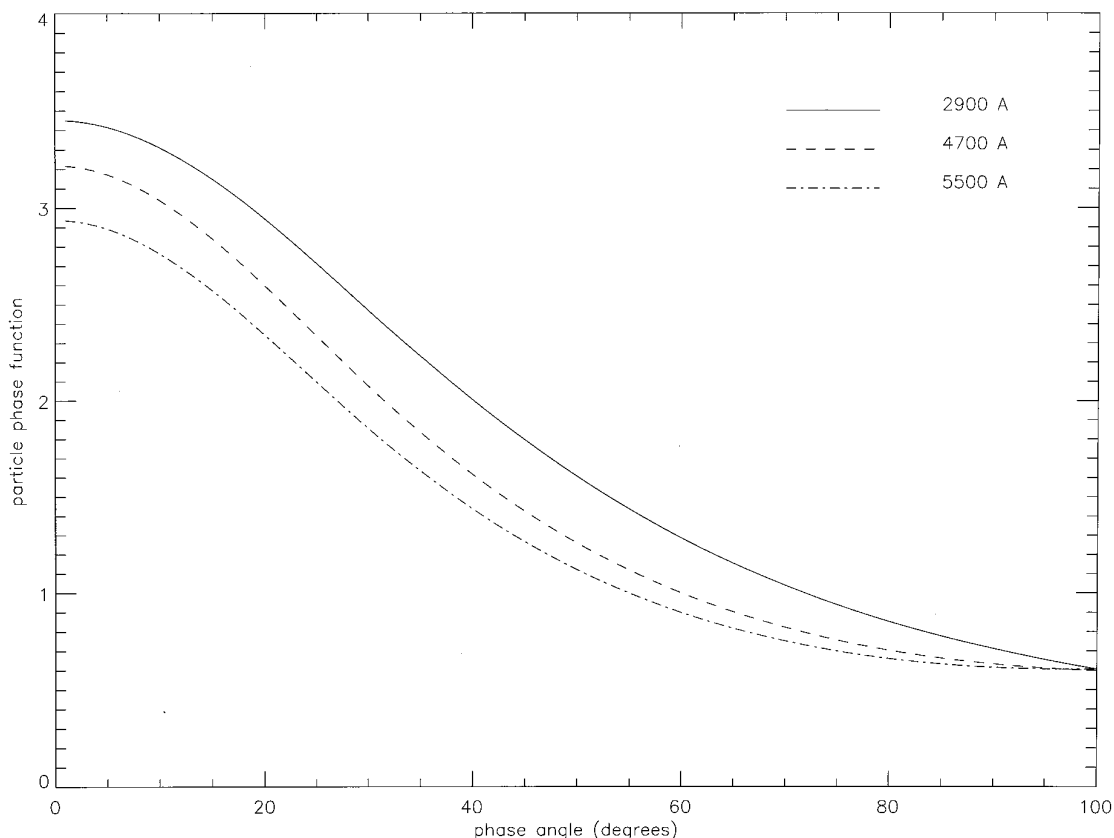


FIG. 3. Derived phase function for Europa's trailing hemisphere at 2900 Å (solid line). Also shown are the phase functions derived by Domingue and Hapke (1992) at 4700 Å (dashed line) and at 5500 Å (dot-dash line). The ultraviolet phase function was derived using Eqs. (1) and (2) in a χ^2 analysis with observations between 20° and 80° phase (the disk-resolved observations discussed in this report in addition to three disk-integrated UVS observations of Europa's trailing hemisphere). The best-fit ultraviolet values of b and c were found to be 0.37 and 1.0, respectively, while Domingue and Hapke (1992) found that $b = 0.430$ and $c = 0.713$ at 4700 Å and $b = 0.443$ and $c = 0.609$ at 5500 Å. Europa's trailing hemisphere becomes gradually more backscattering with decreasing wavelength, likely due to the decrease in mean photon path length.

the roughness parameter for Europa's surface has been determined to be minimal: $\bar{\Theta} = 10^\circ \pm 5^\circ$ (Domingue *et al.* 1991), compared with, for example, $\bar{\Theta} = 24^\circ$ for the lunar highlands (Helfenstein and Veverka 1987). Domingue and Hapke (1992) found the largest value of the surface roughness parameter to be $\bar{\Theta} = 15^\circ$ for any european terrain type measured and that differing disk-resolved european terrains have essentially the same surface roughness parameter. Thus, neglecting the surface roughness parameter in the Hapke photometric function should not affect the relative albedos derived for any location.

We assume, therefore, that neglect of the surface roughness parameter and opposition effect terms nevertheless results in relatively correct albedos (although this assumption may affect the absolute albedo values). It is more likely that individual terrain types have different phase curves which are not accounted for here, which may affect the magnitude (not shape, assuming the phase curve does not vary over the 2100–3200 Å range) of the derived albe-

dos of different terrains. However, any uncertainty incurred by (a) using Eq. (1) to correct observational geometry and/or (b) using the same b and c values for the different terrain types will likely be less than the statistical error on each observation. Demanding that the model fit the data to within 5% results in derived albedos with uncertainties of less than 2%.

Error Analysis

The primary source of error in the resultant single-scatter albedos is the statistical error. The magnitude of the statistical error is dependent on the number of spectra averaged for an observation (outlined in Table I) and on the background radiation noise, which is roughly inversely proportional to the distance (R_J) from Jupiter and follows the magnetospheric charged particle density (see Table II). The error on the signal was derived using

$$\text{error} = \frac{\sqrt{S + 2N}}{\sqrt{xk}}, \quad (4)$$

where x is the number of spectra used in the observation (listed in Table I), k is the smoothing factor (3 or 5), S is the signal, and N is the background radiation noise.

4. RESULTS

Europa's Trailing Hemisphere Particle Phase Function

The trailing hemisphere particle phase function derived using the UVS data is shown in Fig. 3. The function is given by Eq. (2), with best-fit values of b and c of 0.37 and 1.0, respectively, with an estimated uncertainty in b of ± 0.05 . Because the Hapke model (Eq. (1)) assumes isotropic multiple scattering and anisotropic multiple scattering is accounted for in the single-scattering term, the derived values of b and c may actually be upper limits; however, Domingue and Verbiscer (1997) showed that for a three-parameter double-lobed Henyey–Greenstein phase function, accounting for anisotropic multiple scattering produced results similar to those derived accounting for isotropic multiple scattering.

The phase functions derived by Domingue *et al.* (1991) for Europa's trailing hemisphere at visible wavelengths are also shown in Fig. 3, where $b = 0.443$ and $c = 0.609$ at 5500 Å, and $b = 0.430$ and $c = 0.713$ at 4700 Å. The best-fit ultraviolet values of b and c thus continue the trend of Europa's trailing hemisphere becoming more backscattering and less forward-scattering with decreasing wavelength. This is consistent with a shorter path length (Domingue *et al.* 1991), as the shorter wavelength probes less deeply into the particles. The reader is reminded that the ultraviolet phase function was derived using observations in the 20°–80° phase angle range. When future Galileo observations at larger and smaller phase angles are obtained, the phase function will be redetermined; we expect that the c term in particular may be refined when larger phase angle observations are included in this analysis.

Disk-Resolved Albedos

Several resultant albedos are plotted in Fig. 4. Each albedo was derived using Eq. (1) and the number of spectra is indicated in Table I. Statistical error bars (Eq. (4)) are included in each albedo, and the albedos are shown plotted in 18-Å bins to reduce clutter. Each albedo is plotted over the wavelength range in which the error bars were not unreasonably large, generally 2200–3200 Å. For comparison, we show in Fig. 4c the albedo of Europa's disk-integrated leading hemisphere (central longitude 120° W, measured by the UVS on November 4, 1996). Immediately apparent is the fact that the magnitude and shape of the albedo of Europa's surface vary from place to place. On the antijovian hemisphere (Fig. 4a), the albedos are relatively high and red in shape (they increase with increasing wavelength); they have the same shape at three latitudes,

but the magnitude varies. There is a suggestion of a flattening-out of the albedo at longer wavelengths. At the trailing hemisphere apex (Fig. 4b), the albedo is low and relatively flat in shape, with a suggestion of an absorption feature centered near 2800 Å. Thus, Europa's surface is heterogeneous in the ultraviolet. Here we focus on the broad shape of the albedos; smaller possible absorption features will be studied in the future. Figure 5 emphasizes the variations in albedo magnitude and shape by ratioing the albedo of Europa's surface at three trailing hemisphere locations to the disk-integrated leading hemisphere albedo. Regions vary from being brighter and bluer than the leading hemisphere to being much darker than the leading hemisphere, with an absorption feature centered near 2800 Å.

In an attempt to understand how the albedos and the absorption features might be correlated with location on the surface (to see if there is a relationship with exogenic processes), we plot in Fig. 6 the albedo of each location at several wavelengths vs distance from the trailing hemisphere apex (0° N, 270° W) for observations at all latitudes. We also show in Fig. 6 the albedo at each location vs longitude, accounting for latitude, where latitude bins are indicated by various symbols. Figure 6 indicates that, overall, Europa's surface darkens at ultraviolet wavelengths approaching the trailing hemisphere apex. This correlation is generally strongest at the longer wavelengths, as the albedo–longitude slope decreases slightly with wavelength. The slope is the steepest at 2800 Å, where the trailing hemisphere regions have an absorption band center (discussed below). Furthermore, regions toward the antijovian hemisphere (toward 180° W) are certainly brighter than near 270° W, while (despite a relative lack of data) there is an indication that regions toward the jovian hemisphere (toward 360° W) also increase in brightness away from the trailing hemisphere apex.

In addition to the general albedo–longitude trend, we detect variations in albedo that are correlated with the visible brightness of the terrain type. For example, the relatively high albedo at 266° W in Fig. 6b corresponds with the bright rays of the Pwyll crater (E6 SUCOMP01), while the relatively low albedo near 300° W in Fig. 6b corresponds to a very dark mottled terrain region (E4 SUCOMP02).

To determine any relationship between albedo shape and location, we plot in Fig. 7 two albedo ratios (2800/3190 Å and 2500/2800 Å) vs distance from the trailing hemisphere apex and vs longitude. A low 2800/3190 Å ratio, along with a low 2500/2800 Å ratio, means that the region has a red albedo. If the 2500/2800 Å ratio is not as low as the 2800/3190 Å ratio, the albedo tends to flatten out at shorter wavelengths, or to have an absorption band centered near 2800 Å. Figure 7a shows that all regions

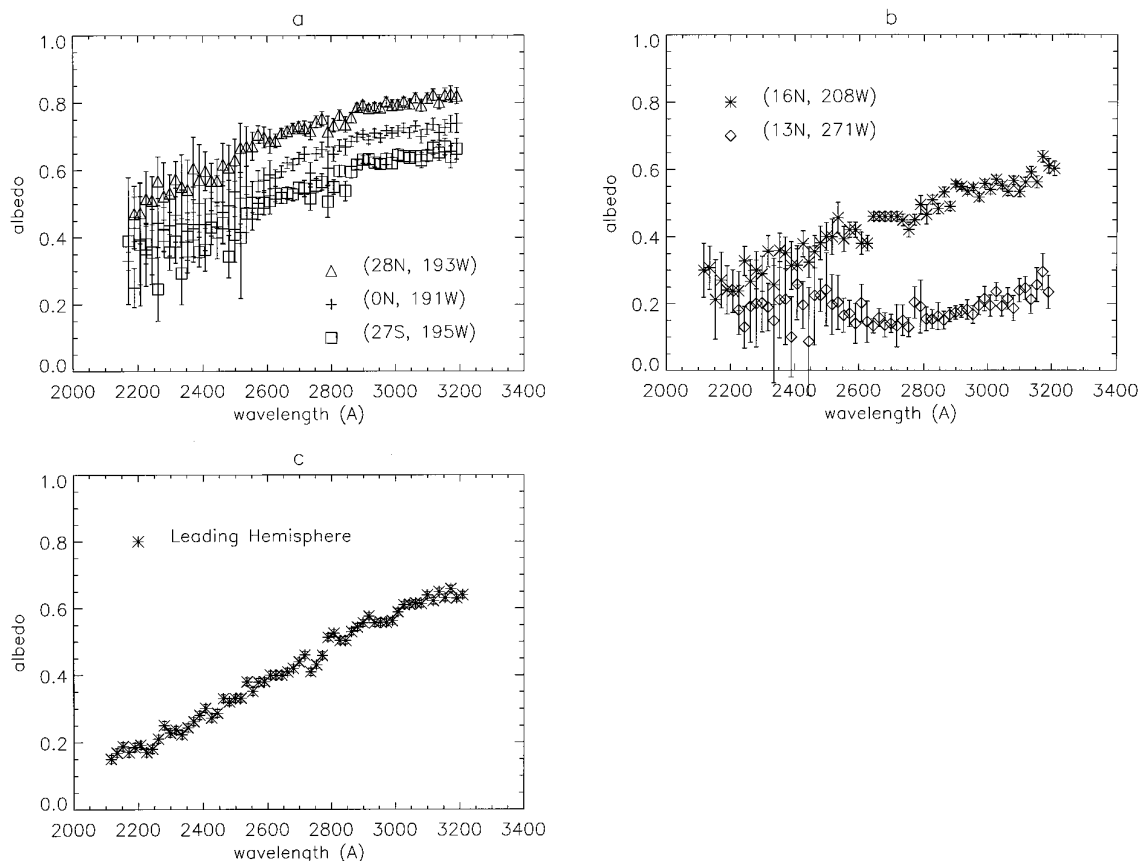


FIG. 4. Albedos of selected regions on Europa's trailing and antijovian hemispheres as measured by the Galileo UVS: (a) regions observed during the FLEXUS observation, (b) regions observed during orbits 4 and 6, and (c) leading hemisphere (120° W central longitude) disk-integrated observation.

generally have red-shaped albedos in the range 2800–3190 Å, with the steepness of the slope increasing toward the trailing hemisphere apex. In the 2500/2800 Å ratio (Fig. 7c), the ratio generally increases toward the trailing hemisphere apex, indicating that near 270° W, albedos flatten out or are blue in the range 2500–2800 Å range. Taking both ratios into account, regions farther from the trailing hemisphere apex have albedos that generally increase with wavelength over the range 2500–3200 Å; regions closer to 270° W have albedos that are flat or blue (increase with decreasing wavelength) at shorter wavelengths and are red toward longer wavelengths—so that overall, they show signs of an absorber.

5. DISCUSSION

Three general factors may contribute to the shape and magnitude of the albedos measured at various locations on Europa's trailing hemisphere. These factors are (1) sublimation, sputtering (due to bombardment by Jupiter's corotating magnetospheric plasma), and redeposition, which

could affect the albedo latitudinally (Sieveka and Johnson 1982), (2) bombardment by Jupiter's corotating magnetospheric plasma, which may erode away the surface, implant ions (inducing an absorption feature), and alter grain size and might affect the albedo longitudinally and latitudinally, with the greatest effect near 0° N, 270° W (Pospieszalska and Johnson 1989), and (3) terrain type observed, generally dependent on endogenic processes. We discuss our results in terms of these three factors.

Albedo Magnitude

Longitude dependence. Figure 6 displays a correlation between albedo and longitude. The albedo decreases between 180° and 270° W and increases again between 270° and 360° W. We see this darkening toward the trailing hemisphere apex occur at all wavelengths between 3200 and 2500 Å, with the effect becoming slightly less drastic with decreasing wavelength. These results are consistent with the Voyager results of McEwen (1986). Johnson *et al.* (1988) found that a decrease in brightness of Voyager data (between 0.59 and $0.35 \mu\text{m}$) toward the trailing hemisphere

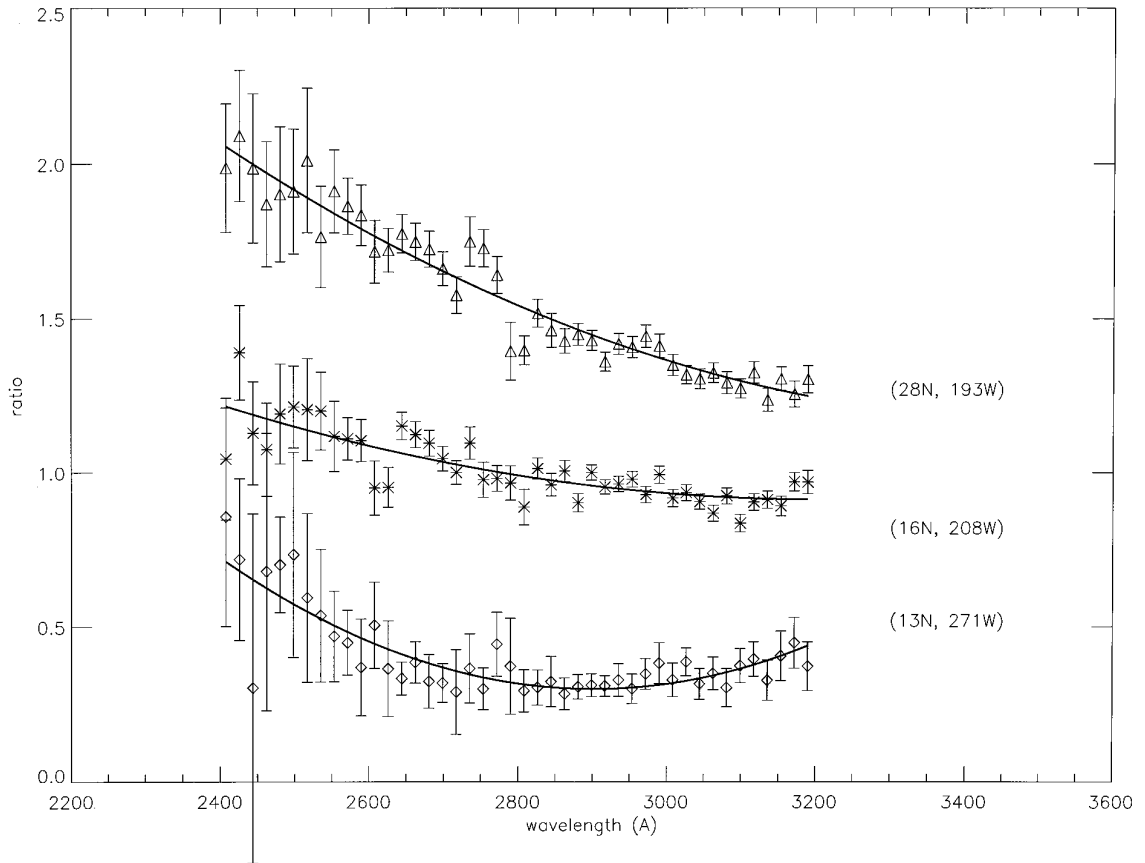


FIG. 5. Albedo ratios. The albedo of three trailing hemisphere (longitude $> 180^\circ$ W) regions (from Fig. 4) are shown ratioed to the leading hemisphere disk-integrated albedo (Fig 4c). Ratios display variations in brightness and absorption depth across the surface and are overplotted with a polynomial fit to emphasize the broad shape of ratios.

apex was due to the larger grain size on the trailing hemisphere, which is a result of the destruction of small particles by magnetospheric bombardment and the relative lack (compared to the leading hemisphere) of meteoritic bombardment, which tends to create small particles.

The fact that we see a slight decrease in the albedo–longitude slope with wavelength is related to the absorber found near the trailing hemisphere apex, which makes the albedos over the entire trailing hemisphere more uniform at shorter wavelengths (see Fig. 4b). This is discussed more below.

Additional observations on the trailing jovian hemisphere (between 300° and 360° W longitude) are needed to confirm the albedo–longitude relationship there. Jovian hemisphere observations will also help identify any dust or sulfur particle implantation from Io. Furthermore, at shorter wavelengths, we see a possible decrease in the relative brightness difference between regions near the trailing hemisphere apex and regions toward the jovian hemisphere. To determine whether this is a real effect, more lower spatial-resolution observations of the jovian

hemisphere are needed. As discussed below, lower spatial-resolution observations may be particularly helpful in determining the overall pattern at ultraviolet wavelengths due to exogenic processes, while higher spatial-resolution observations (which are what we currently have on the jovian hemisphere) reveal more about the small-scale variations in terrain type.

Latitude dependence. Based on the information in the albedo vs longitude plots of Fig. 6, three conclusions may be drawn:

1. The regions in the central latitude bins (20° S to 20° N and 40° S to 20° S) are generally darker at all wavelengths than regions at higher latitudes.

2. The albedos in the 20° N to 40° N latitude bin are higher at most wavelengths than in the 40° S to 20° S bin and are thus not symmetric about the equator, and they do not as strongly follow the albedo–longitude trend of the other central latitude bins. At 2500 \AA , the antijovian hemisphere observations in the 20° N to 40° N latitude bin appear to follow the albedo–longitude trend more than at

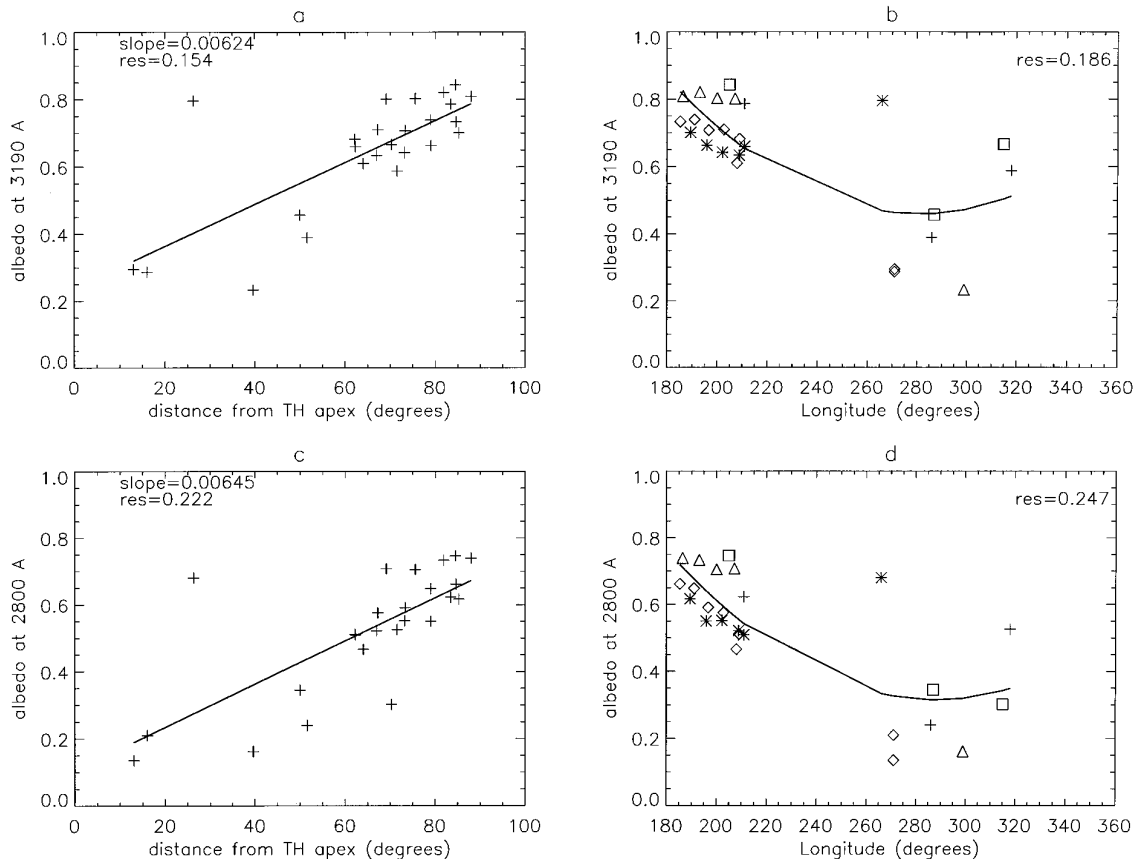


FIG. 6. Plots of albedo vs distance from trailing hemisphere apex (0° N, 270° W) and vs longitude for 3190, 2800, 2600, and 2500 Å. Latitude bins (in albedo vs longitude plots) are designated as follows: + 60° – 40° S, * 40° S– 20° N, diamond 20° S– 20° N, triangle 20° – 40° N, square 40° – 60° N. At all wavelengths, the albedo decreases toward the trailing hemisphere apex. The albedo vs distance from trailing hemisphere apex plots are shown with the best-fit straight line to the data (goodness of fit indicated by residual). The albedo vs longitude plots were better fit with a polynomial fit of degree 2 (rather than a line), indicating that the albedo increases toward both the jovian and antijovian hemispheres.

longer wavelengths. Additional higher latitude observations, particularly near the trailing hemisphere apex, are needed to confirm this.

3. Due to a paucity of observations, it is difficult to detect an albedo–longitude trend in the 60° S to 40° S and 40° N to 60° N latitude bins or to determine definite variations in albedo magnitude at those higher longitudes. However, we can say that these data suggest that the high latitude regions are not brighter or darker, within the statistical error, of each other or of neighboring latitude bins.

These results are consistent with those of McEwen (1986) who mapped the Voyager UV/VIS data to show an elliptical pattern covering the trailing hemisphere. At longer wavelengths, closer to 180° W, the dark pattern does not extend to very high latitudes, as it does near 270° W. Thus, it is not surprising that the albedos in the 20° N to 40° N bin do not decrease with longitude between 180° and 210° W: those regions are not included in the elliptical pattern created by the exogenic process. Closer to 270° W,

even high latitude regions are dark, and moving onto the jovian hemisphere, high latitude regions become brighter before the lower latitude regions do. At 2500 Å, we see that the albedos in the 20° N to 40° N bin on the antijovian hemisphere may begin to decrease with longitude. More observations are needed to confirm this, but this may be the effect of magnetospheric bombardment, which creates a more uniformly dark surface at shorter wavelengths.

These results are consistent with a darkening of the surface by magnetospheric bombardment, which is focused at lower latitudes and at longitudes approaching 270° W. Sieveka and Johnson (1982) showed that, at 270° W, the most erosion of Europa's trailing hemisphere due to corotating ions and fast-ion sputtering should occur at latitudes lower than $\sim 20^{\circ}$, while uniform erosion occurs between $\sim 20^{\circ}$ and $\sim 65^{\circ}$, with less erosion occurring at higher latitudes. The erosion by sputtering thus darkens the surface by uncovering darker material, by destroying small particles, or by creating an absorbing material by interaction between the ions and the water ice.

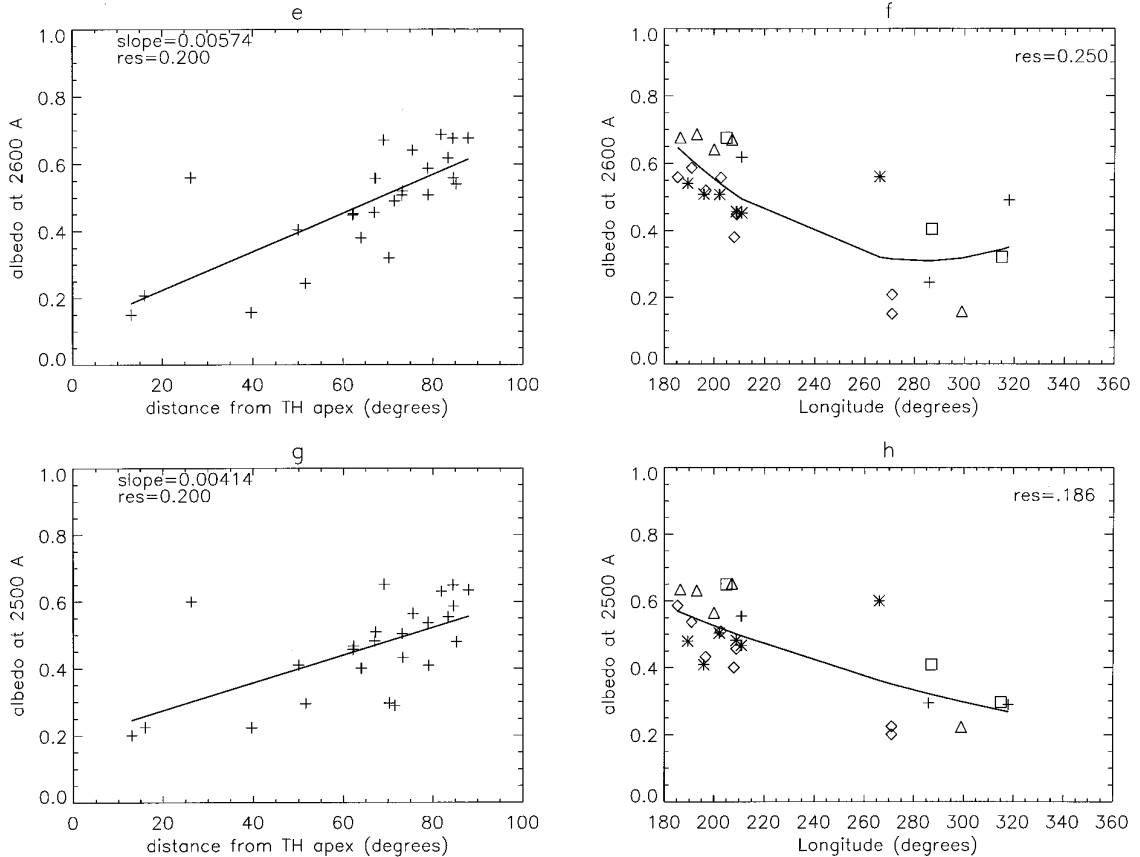


FIG. 6—Continued

Dependence on terrain type. We find that, although the general trend is that the ultraviolet albedo decreases toward the trailing hemisphere apex (due to an exogenic process), the albedo is also sensitive to terrain type (endogenic). The darkest regions at 3190 Å correspond to the dark mottled terrain on the trailing hemisphere. The visibly bright rays of Pwyll crater are bright in the ultraviolet, despite their 266° W location. The brightest albedo was measured near 55° N, 205° W, corresponding to a region of what appears to be pure water ice. We note that a Galileo NIMS observation of Europa (Carlson *et al.* 1996) determined that a high northern latitude region (near 60° N, 270° W) likely consisted of water ice covered by fine-grained water ice. FLEXUS Swath 1 (29° N) covered a region of mostly bright ice with superimposed dark linea, and has correspondingly relatively bright albedos compared to the albedos of FLEXUS Swath 2 and 3 (0° N and 28° S), which covered visibly darker regions.

Because some albedos in Fig. 6 do not strictly obey the albedo–longitude trend, the spatial resolution of these observations needs to be addressed. Some of the observations on the trailing hemisphere were performed at much higher spatial resolution than those observations on the

antijovian hemisphere (namely FLEXUS and TERRA INCOGNITA). The albedo–longitude correlation shown in Fig. 6 is particularly strong in the observations of lower spatial resolution. The observations that had higher spatial resolution resulted in albedos that are more prone to small-scale variations in terrain type.

Are the higher spatial-resolution albedos actually more variable in magnitude, or is this an effect of the phase curve applied to them? The answer is probably a little of both. It is doubtful that, at ultraviolet wavelengths, the entire trailing hemisphere of Europa varies, even at small scales, with the exogenic pattern only. However, it is likely that individual, anomalously bright or dark regions scatter light according to a different phase function than that applied here, so we have not corrected enough.

If we use the lower spatial resolution observations to obtain the large-scale pattern of Europa’s trailing hemisphere albedo variations, we may solve for the phase curves of the “anomalously” bright and dark regions that were measured at higher spatial resolution. Although it is not possible to derive accurate phase curve parameters of each terrain type with this data set, we find that, to agree with the large-scale exogenic pattern, the Pwyll crater rays must

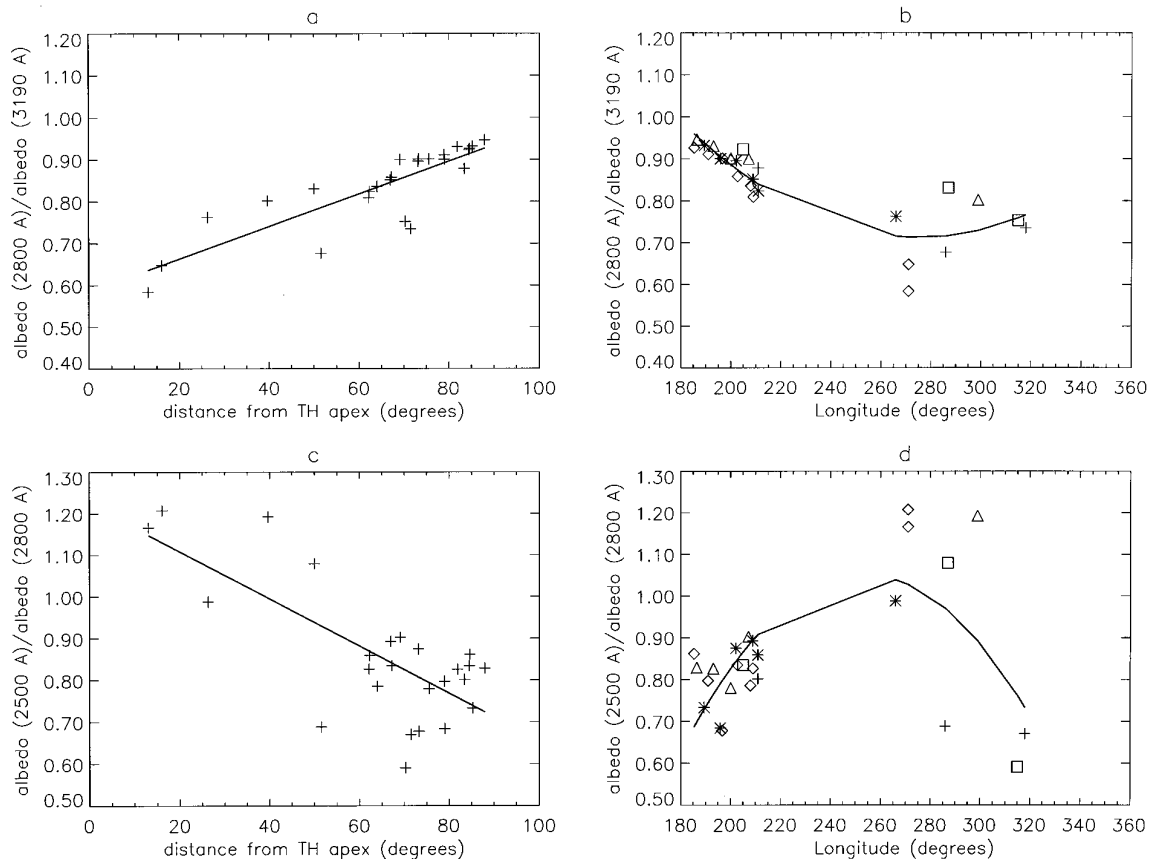


FIG. 7. Albedo ratios vs distance from trailing hemisphere apex and longitude. (a) and (b) 2800/3190 Å, (c) and (d) 2500/2800 Å. Latitude bins are indicated as follows: + 60°–40° S, * 40° S–20° N, diamond 20° S–20° N, triangle 20° N–40° N, square 40°–60° N. Away from the trailing hemisphere apex, albedos are red (low 2800/3190 Å and 2500/2800 Å ratios), while closer to 270° W, albedos have an absorption feature, indicated by a low 2800/3190 Å ratio in combination with a relatively high 2500/2800 Å ratio.

be much less backscattering than the average european trailing hemisphere terrain, with a b value of approximately 0.01. The dark region covered in E4 SUCOMP02 must be much more backscattering than the average surface, with a b value near 0.7. Thus, we conclude that particularly bright and dark areas most likely scatter light according to different phase curves than the “average” phase curve that we used. However, we cannot determine the phase functions of each of these regions except to say the bright regions are probably less backscattering and dark regions are probably more backscattering than the overall trailing hemisphere. McEwen (1986) found that endogenic features were visible despite the exogenic pattern in the Voyager UV data; it is thus probable that, even correctly accounting for phase curves would result in endogenic variations in brightness superimposed on the larger scale exogenic darkening of the surface.

Albedo Shape

Longitude dependence. We detect a correlation between absorption band depth and location on the surface

that is correlated with an exogenic process. Figure 7 shows that, away from the trailing hemisphere apex, albedos are generally red. The 2800/3190 Å and 2500/2800 Å ratios are both less than unity; furthermore, the 2500/2800 Å ratios generally have smaller or similar values to the 2800/3190 Å value, indicating that, if anything, the albedos are flatter toward longer wavelengths than toward shorter wavelengths. Closer to the trailing hemisphere apex, albedos are flatter toward shorter wavelengths, or they have an absorption band (smaller 2800/3190 Å ratios than 2500/2800 Å ratios, and the 2500/2800 Å ratios are close to unity). This change in shape of albedo with longitude is the reason for the decrease in the albedo–longitude slope at shorter wavelengths (Fig. 6). This is a distinct difference from the results of Johnson *et al.* (1988), who showed, using Voyager data in the 0.35- to 0.59- μm bands, that all european regions are red in shape, regardless of longitude. Thus, we find that observations at shorter wavelengths reveal differences in albedo shape with longitude.

Regions on the antiojovian hemisphere are red in both ratios, while regions close to 270° W are red in the 2800/

3190 Å ratio and blue or flat in the 2500/2800 Å ratio. Thus, only the regions closest to 270° W display the absorption band or flattening-out toward shorter wavelengths. This is in contrast to the darkening with longitude of Fig. 6, where the darkening generally occurs at all trailing hemisphere longitudes, with the darkening effect diminishing away from the trailing hemisphere apex.

Latitude dependence. Figure 7 indicates that the deepest absorption bands generally occur at the lower latitudes. This result is consistent with an increased darkening of the surface at lower latitudes due to an exogenic process. It is also notable that none of the three observations at high southern latitudes display a bowl-shaped albedo, while the three high northern latitude observations generally follow the trend of a flat or bowl-shaped albedo near the trailing hemisphere apex and redder albedos away from it. More observations are needed to confirm any band depth–longitude correlation at high latitudes.

We find that, regardless of latitude, the regions on the antijovian hemisphere that adhered strictly to the exogenic ellipse pattern of McEwen (1986) all seem to be red in shape (low values of both ratios). Thus, we find that a more constricted region displays the absorption, compared to the larger region that displays the darkening. Regions far from 270° W longitude darken with longitude, while only regions closer to 270° W display the absorption band.

Dependence on terrain type. The albedo shape (band depth) does not seem to depend upon terrain type. For example, the bright Pwyll crater rays nevertheless display an absorption band or flattening at shorter wavelengths. The darkest regions on the trailing hemisphere also display a strong absorption.

Thus, we conclude that the absorption band is related only to location on the trailing hemisphere and not to terrain type. The absorption occurs near 270° W longitude, while the darkening occurs over a more extended region. We postulate that the corotating ions that impact near 270° W are implanted deep into the ice lattice and interact with the ice to create an absorber, and at the same time they darken the surface by destroying the small ice particles. Those ions that impact the surface farther from 270° W are not as likely to implant themselves deep into the ice, but will sputter ice away to darken the surface. This is related to the bombardment by hot and cold plasma, discussed by Pospieszalska and Johnson (1989). Hot plasma impacts the surface uniformly over the trailing hemisphere and extends evenly to the leading hemisphere. Cold plasma impacts a much more localized region on the trailing hemisphere, with the greatest effect between roughly 235° and 315° W, and with minor effects out to longitudes 20° W on the jovian hemisphere and 160° W on the antijovian hemisphere. We discuss this more below.

What is the Absorber?

The first mention of Europa's trailing hemisphere absorption band near 2800 Å was by Lane *et al.* (1981). Those authors attributed the feature to an S–O bond resulting from magnetospheric S⁺ ions impacting the water ice surface. This was a theoretical explanation, and no laboratory spectra of this S–O interaction existed to compare to the IUE data.

Sack *et al.* (1992) were the first to compare Europa's albedo with laboratory data. They compared the ratio of IUE-measured Europa trailing hemisphere albedo to leading hemisphere albedo with a laboratory-measured spectrum of SO₂ frost grown on water ice and obtained a satisfactory fit. Noll *et al.* (1995) compared a HST-measured global Europa trailing hemisphere spectrum with the SO₂ frost grown on H₂O ice from Sack *et al.* (1992) and also obtained a satisfactory fit. However, these IUE and HST global albedos are measures of a heterogeneous surface. Europa's trailing hemisphere consists of mostly dark, reddish ice, along with linea and some light, purer water ice. In order to understand how these bright and dark areas make up Europa's global albedo, we model the HST-measured albedo (Noll *et al.* 1995), not by comparing with laboratory spectra of homogeneous substances, but by comparing with UVS-measured spectra of dark and light regions on Europa's surface. Figure 8 displays the result, where we have assumed the conversion from single-scatter albedo to geometric albedo as given by Hapke (1993, p. 353). We find that the global spectrum of Europa (measured by HST) is well fit by a mixture of 80% dark material (30% E4 SUCOMP02, 60% ASTERI 2) and 20% bright ice (E4 SUCOMP03). Thus, Europa's disk-integrated trailing hemisphere albedo is dominated by the dark component of the surface, which is located near the trailing hemisphere apex and has an absorption band.

To investigate the nature of the material toward the center of the trailing hemisphere, which has the most absorption, we display in Fig. 9 the ratio a trailing hemisphere dark ice albedo (ASTERI 2) to the global leading hemisphere (Fig. 4c). In Fig. 9a, we compare this ratio with the laboratory measurement of SO₂ frost grown on water ice ratioed to water ice (Sack *et al.* 1992). To make the lab data fit the UVS data, we had to multiply the lab data by a factor of 0.42. Therefore, we conclude that the dark material, which dominates Europa's trailing hemisphere albedo, agrees well with the laboratory spectrum of SO₂ frost grown on water ice. However, because we had to multiply the laboratory spectrum by 0.42 to make it fit the Europa data, Europa's dark ice is much darker than laboratory-measured SO₂ frost grown on water ice. The increased darkening of Europa surface compared to the laboratory spectrum may be due to a larger grain size. We note that the measurement of SO₂ frost on water ice (Sack

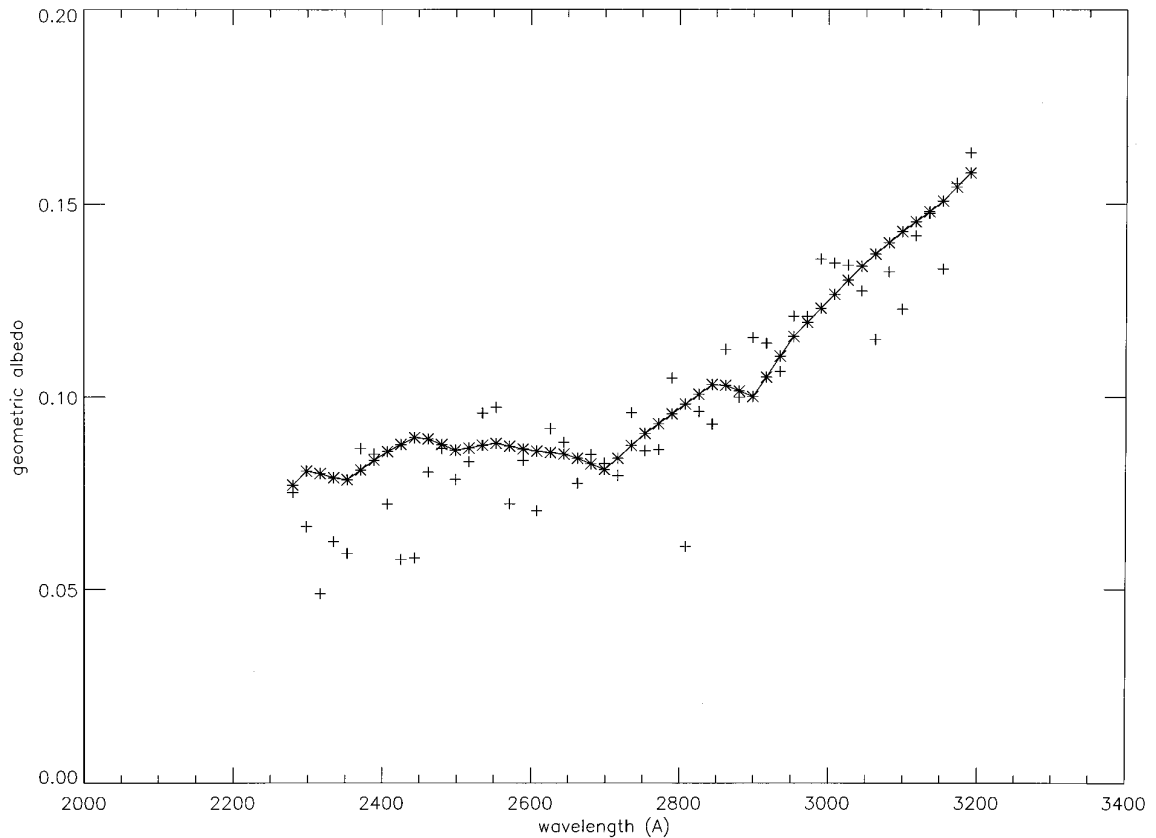


FIG. 8. The HST-measured Europa trailing hemisphere global albedo (*) (from Noll *et al.* 1995) is well fit by a model (+) of UVS-measured albedos, which is made up of a mixture of 80% dark ice (30% E4 SUCOMP02, 60% ASTERI 2) and 20% bright ice (E4 SUCOMP03). The disk-integrated albedo of Europa is thus dominated by the dark ice constituent of the trailing hemisphere..

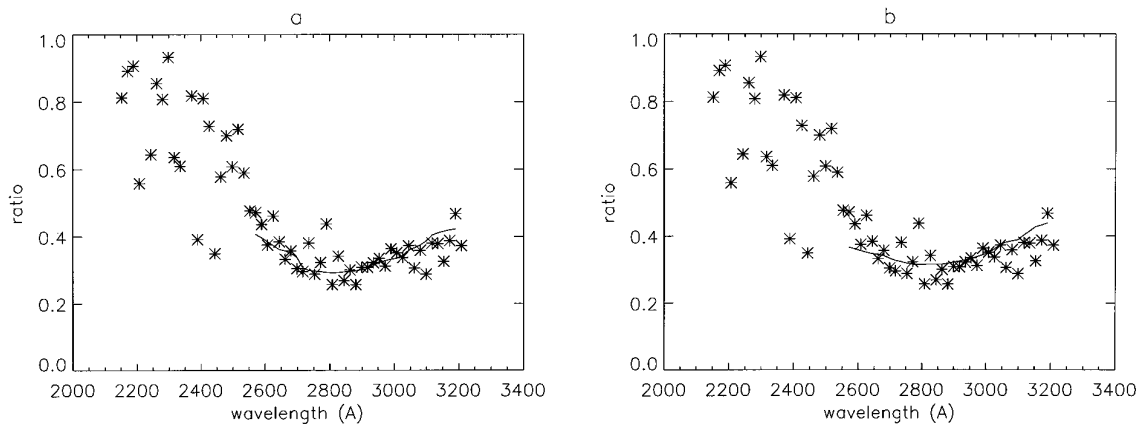


FIG. 9. Ratio of trailing hemisphere dark ice (ASTERI 2) to the global leading hemisphere (*) compared to (a) the laboratory spectrum of SO_2 frost grown on water ice ratioed to pure water ice (Sack *et al.* 1991), multiplied by a factor of 0.42; (b) the laboratory spectrum of trapped OH (Johnson and Quickenden (1997) multiplied by a factor of 0.51. The agreement is slightly better between the data and the SO_2 frost grown on water ice, implying that the dark material on Europa's trailing hemisphere is related to sulfur. However, the UVS data ratio is darker than the laboratory spectra, indicating that Europa's surface is darker than the laboratory spectrum, likely due to large grain size.

et al. 1992) is entirely different from the spectrum of SO₂ frost alone (Nash *et al.* 1980), which is dark and flat at wavelengths shorter than ~ 3100 Å, but at 3100 Å suddenly increases sharply in brightness.

Another material that has an absorption band near 2800 Å is trapped OH due to bombardment of water ice by energetic particles (Johnson and Quickenden 1997). In Fig. 9, we compare the trailing hemisphere dark ice ratioed to the global leading hemisphere to lab spectra from Johnson and Quickenden of trapped OH, but the fits are not quite as good as with the SO₂ frost grown on water ice.

Because sulfur ions are in abundance at Europa's orbit in Jupiter's corotating magnetosphere, and because we obtain a slightly better fit to the data using SO₂ frost grown on H₂O ice compared to the fit obtained using trapped OH, we conclude that sulfur (in some form) is involved in the absorption and that impacting sulfur ions are the source. The absorption is most concentrated in a longitude band up to 90° wide centered on 270° W, where sulfur ions impact the surface and combine with the ice matrix to form the absorber. At longitudes outside this band, corotating ions impact the surface, but are not deeply imbedded, and serve to sputter and darken the ice, but not to create an absorber. A likely scenario, which is in agreement with the Voyager results of Johnson *et al.* (1988), is that impacting cold plasma creates the absorber in a localized region, while impacting hot plasma darkens the surface over the entire trailing hemisphere, with the darkening diminishing away from the trailing hemisphere apex.

6. CONCLUSIONS

Analysis of the disk-resolved (resolutions between 740 and 55 km) spectral ultraviolet data of regions on Europa's trailing and antijovian hemispheres has led to the discovery of variations in ultraviolet albedo, which reveal information about Europa's plasma environment. Our main conclusions are:

1. The ultraviolet phase curve for Europa's trailing hemisphere is in agreement with the longer wavelength results of Domingue *et al.* (1991), where the surface continues to become more backscattering with decreasing wavelength due to the decreased path length of the shorter wavelength. Very dark regions are likely more backscattering, and very bright regions (such as the rays of the crater Pwyll) are likely less backscattering than the overall trailing hemisphere surface.

2. The surface of Europa becomes darker at all wavelengths (2500–3200 Å) toward the trailing hemisphere apex (between 180° and 320° W). The darkening is likely due to impact by Jupiter's corotating magnetospheric plasma, which destroys small particles. The darkening is in agreement with the Voyager results of McEwen (1986),

who found the exogenic pattern to be elliptically shaped. Small-scale variations in albedo magnitude exist on top of the albedo–longitude correlation, due to increased spatial resolution.

3. An ultraviolet absorption, centered near 2800 Å, is present at longitudes near the trailing hemisphere apex. The absorption occurs over a smaller longitude range than the darkening, and we interpret it as being due to bombardment of the surface ice by magnetospheric plasma. According to the bombardment profiles of Pospieszalska and Johnson (1989), cold plasma bombards primarily the $\sim 235^\circ$ – 315° W longitude region and has a minor effect on longitudes extending onto the leading hemisphere. In contrast, hot plasma uniformly bombards both the trailing and leading hemispheres. Our results are consistent with the idea that the darkening over the trailing hemisphere is due to bombardment (and destruction of small ice particles) by hot plasma, while the absorption feature is due to bombardment by, and implantation of, cold plasma (mainly sulfur ions), which both destroy small ice particles to darken the surface and combine with the ice to create an absorber which is spectrally similar to, but darker than, SO₂ frost grown on water ice.

ACKNOWLEDGMENTS

Many thanks to Wendy Calvin and Bob Johnson for insightful reviews. The authors are grateful to Deborah Domingue and Keith Noll for helpful discussions; John Aiello, Kent Tobiska, Stuart Stephens, and Greg Rutz for aid with the observations; Karen Simmons, Jeremy Gebben, and Wendy Sweet for help with the data; James Granahan and the SSI team for the Galileo SSI camera images; Gary Rottman for SOLSTICE solar spectra. Charles Hord is the Principal Investigator of the Galileo UVS experiment and William McClintock performed the instrument calibration.

REFERENCES

- Buratti, B., R. M. Nelson, and A. L. Lane 1988. Surficial textures of the Galilean satellites. *Nature* **333**, 148–151.
- Calvin, W. M., R. N. Clark, R. H. Brown, and J. R. Spencer 1995. Spectra of the icy Galilean satellites from 0.2 to 5 μ m: A compilation, new observations, and a recent summary. *J. Geophys. Res.* **100**, 19,041–19,048.
- Carlson, R., and 39 colleagues 1996. Near-infrared spectroscopy and spectral mapping of Jupiter and the Galilean satellites: Results from Galileo's initial orbit. *Science* **274**, 385–388.
- Domingue, D., and B. Hapke 1992. Disk-resolved photometric analysis of European terrains. *Icarus* **99**, 70–81.
- Domingue, D. L., and A. L. Lane 1997. Europa through the eyes of IUE: Possible decade length spatial variations in the UV. *Geophys. Res. Lett.*, submitted.
- Domingue, D. L., and A. Verbiscer 1997. Re-analysis of the solar phase curves of the icy Galilean satellites. *Icarus* **128**, 49–74.
- Domingue, D. L., B. W. Hapke, G. W. Lockwood, and D. T. Thompson 1991. Europa's phase curve: Implications for surface structure. *Icarus* **90**, 30–42.

- Hamilton, D. P. 1996. Dust from Jupiter's Gossamer ring and the Galilean satellites. *Bull. Am. Astron. Soc.* **28**, 1123.
- Hapke, B. 1981. Bidirectional reflectance spectroscopy. 1. Theory. *J. Geophys. Res.* **86**, 3039–3054.
- Hapke, B. 1993. *Theory of Reflectance and Emittance Spectroscopy*. Cambridge University Press, New York.
- Helfenstein, P., and J. Veverka 1987. Photometric properties of lunar terrains derived from Hapke's equation. *Icarus* **72**, 342–357.
- Hendrix, A. R. 1996. *The Galileo Ultraviolet Spectrometer: In-flight Calibration and Ultraviolet Albedos of the Moon, Gaspra, Ida and Europa*. Ph.D. thesis, University of Colorado.
- Hendrix, A. R., and 13 colleagues 1996. Galileo ultraviolet spectrometer observations of Europa. *Bull. Am. Astron. Soc.* **28**, 1140.
- Horanyi, M. 1996. Charged dust dynamics in the Solar System. *Annu. Rev. Astron. Astrophys.* **34**, 383–418.
- Hord, C. W., and 12 colleagues 1992. Galileo ultraviolet spectrometer experiment. *Space Sci. Rev.* **60**, 503–530.
- Johnson, R. E., and T. I. Quickenden 1997. Photolysis and radiolysis of water ice on outer Solar System bodies. *J. Geophys. Res.* **102**, 10,985–10,996.
- Johnson, R. E., M. L. Nelson, T. B. McCord, and J. C. Gradie 1988. Analysis of Voyager images of Europa: Plasma bombardment. *Icarus* **75**, 423–436.
- Johnson, T. V., L. A. Soderblom, J. A. Mosher, G. E. Danielson, A. F. Cook, and P. Kupferman 1983. Global multispectral mosaics of the icy Galilean satellites. *J. Geophys. Res.* **88**, 5789–5805.
- Kliore, A. J., D. P. Hinson, F. M. Flasar, A. F. Nagy, and T. E. Cravens 1997. The ionosphere of Europa from Galileo radio occultations. *Science* **277**, 355–358.
- Lane, A. L., and D. L. Domingue 1997. IUE's view of Callisto: Detection of an SO₂ absorption correlated to Valhalla Basin and possible torus neutral wind alterations. *Geophys. Res. Lett.* **24**, 1143.
- Lane, A. L., R. M. Nelson, and D. L. Matson 1981. Evidence for sulphur implantation in Europa's UV absorption band. *Nature* **292**, 38–39.
- McEwen, A. S. 1986. Exogenic and endogenic albedo and color patterns on Europa. *J. Geophys. Res.* **91**, 8077–8097.
- Millis, R. L., and D. T. Thompson 1975. UVB photometry of the Galilean satellites. *Icarus* **26**, 408–419.
- Morrison, D., N. D. Morrison, and A. R. Lazarewicz 1974. Four-color photometry of the Galilean satellites. *Icarus* **23**, 399–416.
- Nash, D. B., F. P. Fanale, and R. M. Nelson 1980. SO₂ frost: UV-visible reflectivity and Io surface coverage. *Geophys. Res. Lett.* **7**, 665–668.
- Nelson, M. L., T. B. McCord, R. N. Clark, T. V. Johnson, D. L. Matson, J. A. Mosher, and L. A. Soderblom 1986. Europa: Characterization and interpretation of global spectral surface units. *Icarus* **65**, 129–151.
- Nelson, R. M., A. L. Lane, D. L. Matson, G. J. Veeder, B. J. Buratti, and E. F. Tedesco 1987. Spectral geometric albedos of the Galilean satellites from 0.24 to 0.34 Micrometers: Observations with the International Ultraviolet Explorer. *Icarus* **72**, 358–380.
- Noll, K. S., H. A. Weaver, and A. M. Gonnella 1995. The albedo spectrum of Europa from 2200 Å to 3300 Å. *J. Geophys. Res.* **100**, 19,057–19,059.
- Ockert, M. E., R. M. Nelson, A. L. Lane, and D. L. Matson 1987. Europa's ultraviolet absorption band (260 to 320 nm): Temporal and spatial evidence from IUE. *Icarus* **70**, 499–505.
- Pospieszalska, M. K., and R. E. Johnson 1989. Magnetospheric ion bombardment profiles of satellites: Europa and Dione. *Icarus* **78**, 1–13.
- Rosenbush, V. K., V. V. Avramchuk, A. E. Rosenbush, and M. I. Mishchenko 1997. Polarization properties of the Galilean satellites of Jupiter: Observations and preliminary analysis. *Astrophys. J.* **487**, 402–414.
- Rottman, G. J., T. N. Woods, and T. P. Sparr 1993. Solar-stellar irradiance comparison experiment 1. 1. Instrument design and operation. *J. Geophys. Res.* **98**, 10667.
- Sack, N. J., R. E. Johnson, J. W. Boring, and R. A. Baragiola 1992. The effect of magnetospheric ion bombardment on the reflectance of Europa's surface. *Icarus* **100**, 534–540.
- Sieveka, E. M., and R. E. Johnson 1982. Thermal- and plasma-induced molecular redistribution on the icy satellites. *Icarus* **51**, 528–548.
- Stebbins, J. 1927. The light-variations of the satellites of Jupiter and their application to measures of the solar constant. *Lick Obs. Bull.* **13**, 1.
- Stebbins, J., and T. S. Jacobsen 1928. Further photometric measures of Jupiter's satellites and Uranus, with tests for the solar constant. *Lick Obs. Bull.* **13**, 180–195.